New Research Proposal to Jefferson Lab PAC 29

Deeply Virtual Compton Scattering on the Deuteron with CLAS at 6 GeV

M. J. Amarian[1,2,3], H. Baghdasaryan, S. Bueltmann, G. E. Dodge, G. Gavalian, C. E. Hyde-Wright, H. G. Juengst[2], S. E. Kuhn, J. Lachniet, P. E. Ulmer, L. B. Weinstein

Department of Physics, Old Dominion University Norfolk, VA 23529, USA

J. Ball, P. Bertin, S. Bouchigny, A. Camsonne, R. De Masi, C. Ferdi, M. Garçon, F.-X. Girod, M. Guidal, H.-S. Jo, M. MacCormick, M. Mazouz, B. Michel, C. Muñoz Camacho, S. Niccolai, F. Sabatié[2], E. Voutier

LPC (Clermont) - LPSC (Grenoble) - IPNO (Orsay) - SPhN (Saclay)
CEA/DSM/DAPNIA & CNRS/IN2P3, France

A. Afanasev, H. Avakian, V. Burkert, L. Elouadrhiri[2], R. Niyazov, S. Stepanyan

Jefferson Lab., Newport News, VA 23606, USA

V. Kubarovsky, P. Stoler

Rensselear Polytechnic Institute, Troy, NY 12181, USA

S. Kuleshov, N. Pivnyuk, O. Pogorelko

Institute of Theoretical and Experimental Physics, Moskow, 117259, Russia

[1]Contact person
[2]Co-spokesperson
[3]E-mail: amarian@physics.odu.edu

L. C. Smith

University of Virginia, Charlottesville, VA 22903, USA

D. Müller

Department of Physics and Astronomy, Arizona State University, Tempe, AZ 85287, USA

K. Hafidi

Argonne National Laboratory, Argonne, IL 60439, USA

And the CLAS Collaboration

December 8, 2005

Abstract

We propose to measure coherent Deeply Virtual Compton Scattering (DVCS) on a liquid deuterium target using CLAS detector with polarized 6 GeV incident electron beam. In addition to the standard CLAS configuration the experiment requires the inner calorimeter and the solenoidal target magnet.

Our beam time request is 30 days at luminosity of $1.5 \times 10^{34}/cm^2/\mathrm{s}$.

The experiment will measure the beam-spin asymmetry on unpolarized deuterons (A_{LU}). This asymmetry is dominated by the interference between the Bethe-Heitler and DVCS amplitudes.

For the spin-1 target there are nine GPDs of which three contribute to the proposed beam-spin asymmetry measurement. At four-momentum transfer between initial and final state deuteron $-t > 0.2$ GeV^2 the GPD H_3 (related to the quadrupole form-factor) dominates the model estimates of the coherent A_{LU}.

The experiment will have a coverage of $0.1 < x_{Bj} < 0.3$ and $0.15 < -t < 1$ GeV^2 for $Q^2 > 1$ GeV^2.

Contents

1 Preface **4**

2 Introduction **4**

3 Nuclear Targets **6**
3.1 Coherent DVCS on a Deuteron Target 6
3.1.1 Formalism 7
3.1.2 Beam Spin Asymmetry 9
3.2 DVCS on Nuclei 10

4 Existing Experimental Data for DVCS on Nuclei **12**
4.1 HERMES experiment 12
4.2 CLAS E6 analysis 14

5 Theoretical Calculations and Projected Physics Results **17**

6 Experimental DVCS Setup in Hall B **21**
6.1 The DVCS CLAS configuration 21
6.1.1 Detectors 21
6.1.2 Møller electron shielding 22
6.1.3 Target 23
6.1.4 Inner calorimeter 24
6.1.5 CLAS modifications 25
6.2 Trigger, data aquisition, online monitoring 25
6.3 Calibration 27
6.4 IC monitoring 28
6.5 Event identification, reconstruction 28

7 Simulations and Count Rates **30**

8 Summary **33**

9 Acknowledgement **33**

1 Preface

We propose to perform a measurement of Deeply Virtual Compton Scattering (DVCS) on the deuteron with CLAS at 6 GeV. This measurement will be a first step to extend DVCS on a nucleon, to the nuclei with different spin and atomic number, to address some of the most fundamental questions in hadronic and nuclear physics, including

- Partonic structure of spin-$\frac{1}{2}$, spin-1 and spin-0 targets
  - modifications of unpolarized and polarized Generalized Parton Distributions H, $\tilde{\mathrm{H}}$ depending on the spin of the target using *coherent* DVCS on nuclei when the nucleus remains intact
  - distributions of quarks and gluons in nuclei and off-forward EMC effect
- the behavior of nuclei
  - structure and dynamics of the deuteron
  - nucleon-nucleon short range correlations
  - nucleon distortion in the nuclear medium

The present proposal to PAC29 focuses on the case of coherent DVCS on the deuteron.

2 Introduction

Electroproduction of real photons at high momentum transfer, called Deeply Virtual Compton Scattering (DVCS) [MUEL94], is one of the cleanest ways to access non-forward matrix elements of any hadron and nuclei parameterized via Generalized Parton Distributions (GPDs). Handbag diagram for DVCS is shown in Fig. 1. The recent progress in this direction is due to theoretical developments [JI97, RADY96] of GPD formalism and emergence of experimental data from a new generation of facilities at DESY and JLab exploiting polarization and/or the charge of incoming lepton beams [HERM01, STEP01] to get access to the DVCS process at the *amplitude level*. The measurement of DVCS at *cross section level* was performed by

H1 [H105] and ZEUS [ZEUS03] collaborations at very high energies and Q^2, accessible at the HERA e-p collider at DESY.

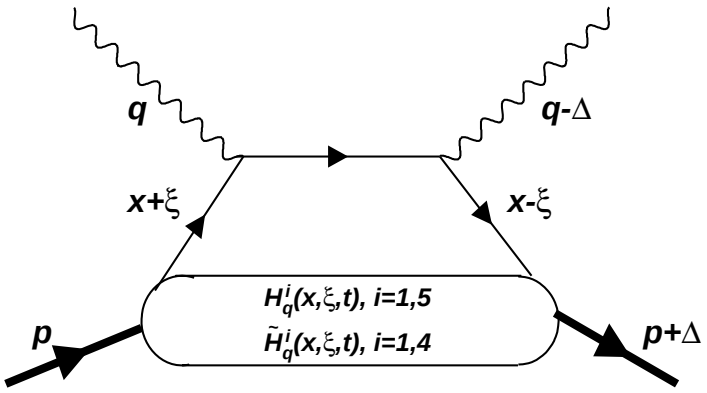

Figure 1: "Handbag" diagram for DVCS. In the $ed \to ed\gamma$ reaction, the DVCS amplitude interferes with the Bethe-Heitler amplitude.

The GPDs shed light on new aspects of the hadrons' internal structure that have not been addressed in the inclusive and semi-inclusive lepton scattering measurements that allowed unraveling forward polarized and unpolarized structure functions. First of all, processes such as DVCS and exclusive meson production extend known structure functions that vanish in the forward limit when four-momentum transfer between initial and final target hadron vanishes. It is shown that depending on the spin of the target one can get a variety of additional structure functions [CANO04]. Theoretically it is proven that the measurement of all these functions will allow eventually to map out the partonic density of nucleons and nuclei and get a three-dimensional picture of these objects. This means that we are facing a dramatic improvement in our understanding of the internal structure of almost all visible matter. It is even possible to make holographic images of hadrons and nuclei at the femtophotographic level.

As a by-product we will also measure incoherent DVCS on the deuteron. In incoherent scattering, the DVCS amplitude is dominated by the proton and neutron GPDs. In addition, the largest contribution to the proton comes from H and the largest contribution to the neutron comes from E. It is worth

mentioning that the first moment (with respect to x) of $H + E$ is equal to the total contribution (spin plus orbital angular momentum) of quarks to the nucleon spin, via a Ji sum rule [JI97].

Until now our knowledge about the density distribution of nuclear matter is based essentially on Hofstadter's famous measurements of charge form factors through elastic scattering of electrons on nuclei [HOFS57].

We can now image the quark density in impact parameter space (or a related Wigner function) as a function of the light-cone momentum fraction of the quark[BURK02, JI04].

On a partonic level, we lack understanding of the modification of quark and gluon distributions in nuclei. The famous nuclear EMC effect remains still to be fully understood. More complex studies of GPDs in nuclei both via coherent and incoherent DVCS are ways to study this effect in a multi-dimensional space and measure a quark level effect in the nuclear media.

3 Nuclear Targets

3.1 Coherent DVCS on a Deuteron Target

The deuteron, being the lowest multinucleon system, is a very special nucleus. It plays a crucial role in a chain of nucleosynthesis and formation of almost all visible matter, and its primordial astrophysical abundance is one of the most sensitive tools constraining the baryon to photon ratio in the universe.

In a last few decades the deuteron has received enormous attention both from theory and experiment as well. However, many questions related to the binding energy, Fermi motion, shadowing, meson exchange currents and partonic structure remain partially or completely open.

Deep-inelastic scattering processes in the deuteron have been used mainly as the source of information on unpolarized and polarized distributions of a neutron in a forward limit. With the advent of DVCS it became possible to study GPDs of a deuteron as a whole leaving it intact in a final state. Due to the fact that it is a spin-1 object there are entirely new functions appearing which could give us a deeper understanding of this nucleus in terms of its fundamental degrees of freedom. The 9 GPDs for a spin-1 object have been given in [BERG01] and their properties have been discussed in detail in [KIRC03].

3.1.1 Formalism

Let us now consider the spin-1 target in more detail. The hadronic current

$$J_\mu = -\epsilon_2^\star \cdot \epsilon_1 P_\mu G_1 + (\epsilon_2^\star \cdot P\epsilon_{1\mu} + \epsilon \cdot P\epsilon_{2\mu}^\star)G_2 - \epsilon_2^\star \cdot P\epsilon_1 \cdot P\frac{P_\mu}{2M^2}G_3 \quad (1)$$

is given by three electromagnetic form factors $G_i(\Delta^2)$ with $i = 1,2,3$, where $\epsilon_{1\mu}$ ($\epsilon_{2\mu}$) denote the three polarization vectors for the initial (final) hadron.

The DVCS hadronic tensor is given by the time-ordered product of the electromagnetic current $j_\mu j_\nu$, which is sandwiched between hadronic states with different momenta. In LO of perturbation theory and at twist-two accuracy it reads [BELI01]

$$\begin{aligned} T_{\mu\nu}(\xi, \Delta^2, \mathcal{Q}^2) &= \frac{i}{e^2}\int dx\, e^{ix\cdot q}\langle P_2|Tj_\mu(\frac{x}{2})j_\nu(\frac{-x}{2})|P_1\rangle \quad (2)\\ &= -\mathcal{P}_{\mu\sigma}g_{\sigma\tau}\mathcal{P}_{\tau\nu}\frac{q\cdot V_1}{P\cdot q} - \mathcal{P}_{\mu\sigma}i\epsilon_{\sigma\tau q\rho}\mathcal{P}_{\tau\nu}\frac{A_{1\rho}}{P\cdot q}\ , \end{aligned}$$

where the projection operator $\mathcal{P}_{\mu\nu} = g_{\mu\nu} - \frac{q_{1\mu}q_{2\nu}}{q_1\cdot q_2}$ ensures gauge invariance. For convenience we introduced the scaling variable $\xi \approx \frac{x_A}{2-x_A}$. At twist-two level the amplitudes V_1 and A_1 can be decomposed in a complete basis of nine Compton Form Factors (CFFs). Adopting the notation of [BERG01], they read in the vector case

$$\begin{aligned} V_\mu = {} & -\epsilon_2^\star \cdot \epsilon_1 P_\mu \mathcal{H}_1 + (\epsilon_2^\star \cdot P\epsilon_{1\mu} + \epsilon_1 \cdot P\epsilon_{2\mu}^\star)\mathcal{H}_2 - \epsilon_2^\star \cdot P\epsilon_1 \cdot P\frac{P_\mu}{2M^2}\mathcal{H}_3 + \quad (3)\\ & (\epsilon_2^\star \cdot P\epsilon_{1\mu} - \epsilon_1 \cdot P\epsilon_{2\mu}^\star)\mathcal{H}_4 + \left(\frac{2M^2\left(\epsilon_2^\star \cdot q\epsilon_{1\mu} + \epsilon_1 \cdot q\epsilon_{2\mu}^\star\right)}{P\cdot q} + \frac{\epsilon_2^\star \cdot \epsilon_1}{3}P_\mu\right)\mathcal{H}_5\ , \end{aligned}$$

and in the axial-vector case

$$\begin{aligned} A_\mu = {} & i\epsilon_\mu\epsilon_2^\star\epsilon_1 P\tilde{\mathcal{H}}_1 - \frac{i\epsilon_{\mu\Delta P\epsilon_1}\epsilon_2^\star \cdot P + i\epsilon_{\mu\Delta P\epsilon_2^\star}\epsilon_1 \cdot P}{M^2}\tilde{\mathcal{H}}_2 - \quad (4)\\ & \frac{i\epsilon_{\mu\Delta P\epsilon_1}\epsilon_2^\star \cdot P - i\epsilon_{\mu\Delta P\epsilon_2^\star}\epsilon_1 \cdot P}{M^2}\tilde{\mathcal{H}}_3 - \frac{i\epsilon_{\mu\Delta P\epsilon_1}\epsilon_2^\star \cdot q + i\epsilon_{\mu\Delta P\epsilon_2^\star}\epsilon_1 \cdot q}{q\cdot P}\tilde{\mathcal{H}}_4\ , \end{aligned}$$

where $\frac{1}{\mathcal{Q}}$-power suppressed effects have been neglected. The remaining logarithmical $\mathcal{Q}$-dependence is governed by pertubation theory.

The CFFs in the above equations are given by a convolution of perturbatively calculable coefficient functions $C^{(\pm)}$ and twist-two GPDs via

$$\mathcal{H}_k(\xi,t) = \sum_{i=u,\ldots} \int_{-1}^{1} dx\, C_i^{(-)}(\xi,x) H_k^i(x,\eta,t)_{|\eta=-\xi}, \quad for\ k=\{1,\ldots,5\} \quad (5)$$

$$\tilde{\mathcal{H}}_k(\xi,t) = \sum_{i=u,\ldots} \int_{-1}^{1} dx\, C_i^{(+)}(\xi,x) \tilde{H}_k^i(x,\eta,t)_{|\eta=-\xi}, \quad for\ k=\{1,\ldots,4\} \quad (6)$$

For each quark species i we have nine GPDs. The two sets $\{H_1^i,\ldots,H_5^i\}$ and $\{\tilde{H}_1^i,\ldots,\tilde{H}_4^i\}$ are defined by off-forward matrix elements of vector and axial-vector light-cone operators.

Sum rules relate these GPDs to the usual deuteron form factors:

$$\begin{aligned} \int_{-1}^{1} dx H_i(x,\xi,t) &= G_i(t) \qquad (i=1,2,3), \\ \int_{-1}^{1} dx \tilde{H}_i(x,\xi,t) &= \tilde{G}_i(t) \qquad (i=1,2)\ , \end{aligned} \quad (7)$$

or lead to a null average:

$$\begin{aligned} \int_{-1}^{1} dx H_4(x,\xi,t) &= \int_{-1}^{1} dx \tilde{H}_3(x,\xi,t) = 0\ , \\ \int_{-1}^{1} dx H_5(x,\xi,t) &= \int_{-1}^{1} dx \tilde{H}_4(x,\xi,t) = 0\ . \end{aligned} \quad (8)$$

The form factors (G_1,G_2,G_3) used above are related with the usual charge monopole, G_C, magnetic dipole, G_M and charge quadrupole, G_Q in the following way:

$$\begin{aligned} G_1(t) &= G_C(t) - \frac{2}{3}\eta G_Q(t) \\ G_2(t) &= G_M(t) \\ (1+\eta)G_3(t) &= G_M(t) - G_C(t) + \left(1+\frac{2}{3}\eta\right) G_Q(t) \end{aligned} \quad (9)$$

with $\eta = -t/(4M_d^2)$. The normalizations of these form factors read:

$$G_C(0) = 1, \quad G_M(0) = \mu_d = 1.714, \quad G_Q(0) = Q_d = 25.83 \quad (10)$$

Note the large size of the quadrupole form factor.

In the forward limit, the functions H_1, $\tilde{H}_1$ and $\mathcal{H}_5$ represent unpolarized, polarized and tensor structure functions F_1, g_1 and b_1 respectively. The following relations link GPDs and parton densities in the deuteron,

$$\begin{aligned} F_1 \simeq H_1(x,0,0) &= \frac{q^1(x)+q^{-1}(x)+q^0(x)}{3}\,, \\ b_1 \simeq H_5(x,0,0) &= q^0(x) - \frac{q^1(x)+q^{-1}(x)}{2}\,, \\ g_1 \simeq \tilde{H}_1(x,0,0) &= q^1_\uparrow(x) - q^{-1}_\uparrow(x) \end{aligned} \tag{11}$$

for $x > 0$. The superscripts are the target spin projection, and the subscripts are the quark spin projections. The corresponding relations for $x < 0$ involve the antiquark distributions at $-x$, with an overall minus sign in the expressions for H_1 and H_5.

The functions $\{H_2,\ H_3,\ H_4\}$ and $\{\tilde{H}_2,\ \tilde{H}_3,\ \tilde{H}_4\}$ are inaccessible in a forward limit, but do not vanish by themselves and provide new information.

3.1.2 Beam Spin Asymmetry

The beam spin asymmetry A_{LU} is defined as

$$A_{LU} = \frac{d\sigma\uparrow(\phi) - d\sigma\downarrow(\phi)}{d\sigma\uparrow(\phi) + d\sigma\downarrow(\phi)}. \tag{12}$$

The arrows refer to the longitudinal spin projections of the incoming electrons. This asymmetry is dominated by the DVCS·BH interference divided by the Bethe-Heitler cross section. For a spin-1 object, such as the deuteron, we can access the linear combination of $\mathcal{H}_1$, $\mathcal{H}_3$ and $\mathcal{H}_5$ directly through the measurement of the beam-spin asymmetry A_{LU} in the reaction $l^\pm(k)A(P_1) \to l^\pm(k\prime)A(P_2)\gamma(q_2)$. As shown in [KIRC03],

$$\begin{aligned} A_{LU}(\phi) \propto\ & \frac{x_A(2-y)\sqrt{\frac{\Delta^2_{min}-\Delta^2(1-y)}{\mathcal{Q}^2}}}{2-2y+y^2} \times \\ & \Im m \frac{2G_1\mathcal{H}_1 + (G_1-2\tau G_3)(\mathcal{H}_1-2\tau\mathcal{H}_3) + \frac{2}{3}\tau G_3\mathcal{H}_5}{2G_1^2+(G_1-2\tau G_3)^2}\sin(\phi) \end{aligned} \tag{13}$$

where $\mathcal{Q}^2 = -q_1^2$, $q_1 = k - k'$, $\tau = \Delta^2/(4A^2M_N^2)$, $y = \nu/E_e$ is a fraction of beam energy E_e carried by a virtual photon, and $G_i(\Delta^2)$ are the form factors

with $i = 1, 2, 3$ (Eq. 9). The form factors $G_i(\Delta^2)$ can be parametrized from elastic electron deuteron scattering [GARC01, GILM01].

The measurement of $\mathcal{H}$ with data from DVCS on the proton and incoherent production on the deuteron will define $\mathcal{H}_1$ in good approximation. $\mathcal{H}_5$ is constrained by the measurement of b_1^d of the deuteron [RIED05].

In section 5 we show that our measurement of A_{LU} will have strong sensitivity to $\mathcal{H}_3$. This provides access to the partonic structure related to the charge quadrupole form factor in an unsuppressed way as can be seen from Eq. 9.

DVCS on the deuteron gives for the first time access to the partonic structure of the deuteron as a whole.

3.2 DVCS on Nuclei

For the sake of completeness and in order to outline recent developments in this field we give a brief overview of DVCS not only on a deuteron, but on a nuclei in general. We would like to make it clear that not only *coherent* DVCS, but also *incoherent* DVCS has been in the focus of recent theoretical papers as a valuable source of a new information about modifications of the nucleon's partonic structure in a nuclear medium and related problems.

In [POLY03] it was argued that by studying nuclear DVCS one can get access to GPDs that carry information about spatial distribution of forces experienced by quarks and gluons inside hadrons. Hard exclusive electroproduction of photons opens a possibility for direct "measurements" of strong forces in different parts of nucleons and nuclei. DVCS measurements give us a tool for systematic studies of properties of quark-gluon matter inside hadrons such as distributions of energy, angular momentum, pressure, shear forces etc..

In [STRI03] ratios of single-spin asymmetries and lepton charge asymmetries measured in nuclei to the same asymmetries measured on the nucleon have been discussed. It was shown that while for coherent scattering this ratio remains roughly proportional to $\frac{A}{Z} \approx 2$ the same ratio for incoherent scattering tends to decrease versus four-momentum transfer between initial virtual photon and produced real photon. These studies have been later extended to the case of a future eA collider and shown to be a powerful tool to unravel quark-gluon structure of the nuclei [STRI04].

The relevance of measuring GPDs of nuclei is stressed and microscopic calculation of unpolarized quark distribution of ^3He nucleus is performed in [SCOP04]. He finds that in impulse approximation Fermi motion and binding effects evaluated by modern potentials are larger in the forward case and very sensitive to the details of the nuclear structure at short distances. And then clear predictions for the off-forward EMC effect were made.

More recently a series of papers (see [LIUT05] and references therein) discussed nuclear DVCS. Within a microscopic calculation the contributions of both, coherent and incoherent deeply virtual Compton scattering from a spin-0 nucleus have been estimated. Although the discussion is valid for any nucleus, more detailed studies have been performed for a ^4He target. It has been shown that the x-distribution of the ratio of functions $H(x,t)$ is more sensitive to the off-shell effects in nuclei than in the forward limit.

This proposal covers only the deuteron case. We consider it a first step towards DVCS on nuclei at JLab at 6 and 12 GeV, and in a future electron-ion collider.

4 Existing Experimental Data for DVCS on Nuclei

4.1 HERMES experiment

So far the only existing experimental data for DVCS on nuclei have been presented by the HERMES Collaboration. The HERA 27.6 GeV polarized positron and electron beam was scattered off polarized and unpolarized deuterium and spin-0 neon gas targets [AMAR00, ELLI03, KRAU05]. The results of an inclusive measurement for the beam spin asymmetry A_{LU} on deuteron and neon targets are shown in Fig. 2. A fit to the function $P_1 + P_2 \sin\phi + P_3 \sin 2\phi$ for the data on the deuteron target results in a beam spin asymmetry $P_2 = -0.15 \pm 0.03(stat) \pm 0.03(sys)$. However from Monte Carlo studies it was concluded that integrated over t, the contribution of coherent scattering is negligible and even at very low $-t < 0.1 GeV^2$ contribution of coherent and incoherent scatterings are comparable [KRAU05]. On the other hand, the contribution of coherent scattering at $-t < 0.1 GeV^2$ on neon is dominant [HAAN05]. Currently the HERMES experiment has installed a recoil detector [KRAU05] with a good capability to detect the recoil proton and deuteron and will start data taking in 2006.

Besides the HERMES experiment only the JLab Hall-A collaboration has performed measurement of DVCS on the deuteron target, however the main goal of this experiment was the extraction of the neutron GPDs and it was not designed for and did not have a capability to detect recoil deuteron.

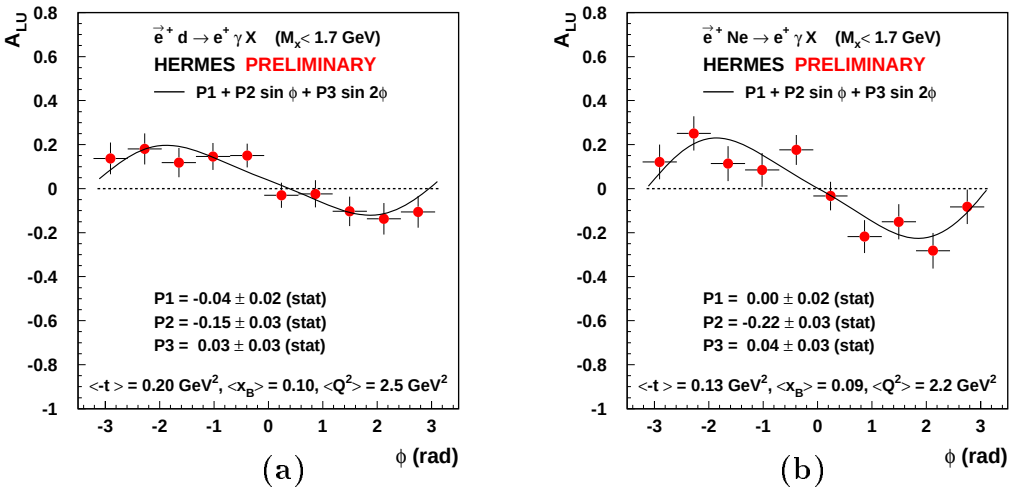

Figure 2: Beam spin asymmetry A_{LU} for $e^{\pm}d \to e^{\pm}\gamma X$ with unpolarized deuteron (a) and $e^{\pm}Ne \to e^{\pm}\gamma X$ (b) from HERMES, inclusive measurement [ELLI03, KRAU05].

4.2 CLAS E6 analysis

A fraction of the CLAS E6 data was taken at an electron beam energy $E_e = 5.75$ GeV with a deuterium target. An analysis of these E6 data with the goal of identifying and analyzing coherent deuteron electroproduction is in progress. The preliminary results for the beam spin asymmetry A_{LU} measurement are encouraging. They show experimental evidence of coherent DVCS on the deuteron.

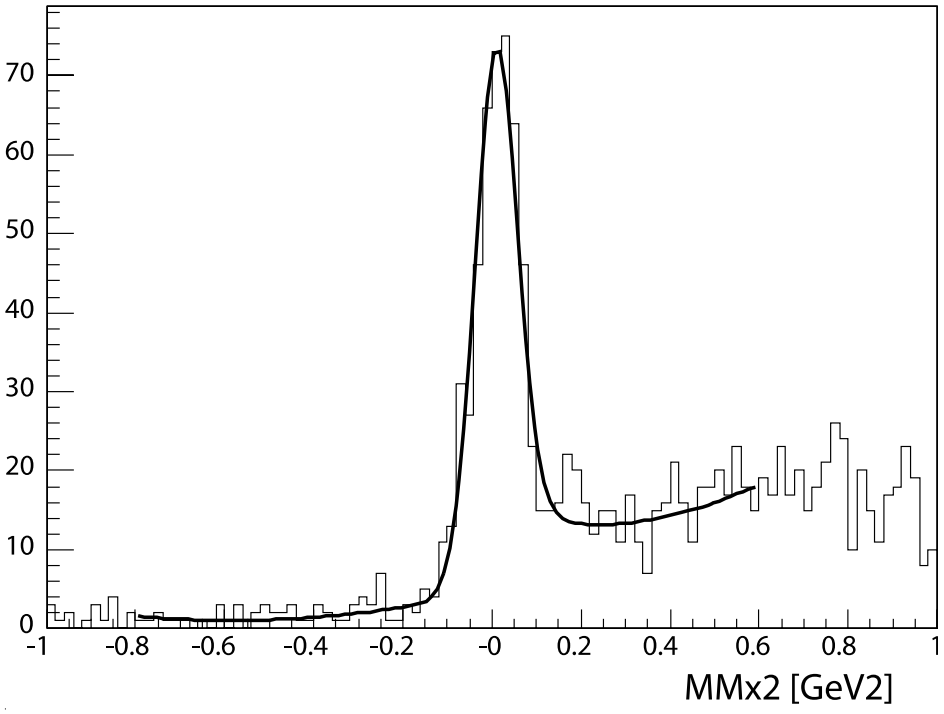

Figure 3: Missing mass m_X^2 of e d $\rightarrow$ e d X in GeV^2 for the ϕ bin averaged around 40° along with a skewed-gaussian + polynomial fit.

For the analysis events with only an electron and a deuteron in the final state were selected. Various cuts on the reconstructed track parameters and particle identification ensure a good signal to background ratio for the selected sample. The expected missing photon is identified by the missing mass method. Fig. 3 shows a peak centered around 0 for the missing mass.

Data are then separated into ϕ bins. The numerator of the asymmetry, containing the cross-section difference, is computed directly by subtracting contributions from both helicities in the missing-mass spectra around the mass equal 0 area. This allows for an automatic background subtraction since the cross-section difference showed no signal outside of this peak.

Finally, the denominator of the asymmetry is computed for each ϕ bin by performing a fit of a skewed gaussian plus polynomial to the missing mass spectra and deducing the total number of events around the missing mass equal 0 peak. The fitted function is illustrated in Fig. 3 for one ϕ bin averaged around $40°$.

The calculated beam spin asymmetry A_{LU} for every bin in ϕ is presented in Fig. 4. The beam spin asymmetry corresponds to the average kinematic point
$< x_A >= 0.1$, $< Q^2 >= 1.7$ GeV^2, $< -t >= 0.3$ GeV^2.

The analysis is in an early stage. Two corrections have to be applied later. First, the beam polarization was not well measured during E6, since the experiment E6 initially did not require it. The average polarization is estimated to be around 60% and requires further analysis. Second, the current lack of π^0 subtraction needs to be addressed, too.

Nevertheless, it is rather clear that a large asymmetry exists in the coherent deuteron DVCS channel and that a dedicated experiment is feasible and needed for further investigation.

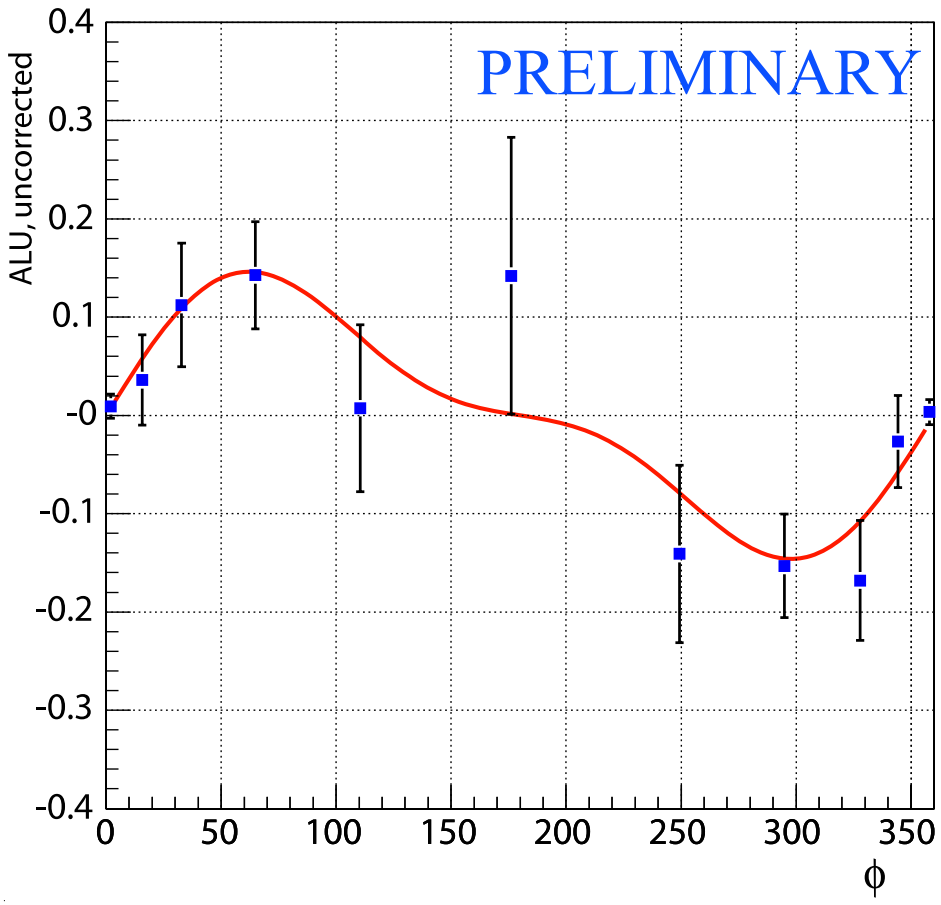

Figure 4: Uncorrected beam spin asymmetry A_{LU} as a function of ϕ for $< x_A >= 0.1$, $< Q^2 >= 1.7$ GeV^2, $< -t >= 0.3$ GeV^2. The curve is a fit of the data with the function $\alpha \sin\phi + \beta \sin 2\phi$.

5 Theoretical Calculations and Projected Physics Results

Theoretical models [KIRC03] were used to predict the beam spin asymmetry A_{LU}. The kinematical parameters have been adjusted for CLAS. The results shown in Fig. 5 were calcuated for fixed JLab beam energy $E_e = 6$ GeV, and, in average, $x_B = 0.2$, $\mathcal{Q}^2 = 1.5$ GeV^2, and $\Delta^2 = -0.25$ GeV^2, with $x_B = \frac{Q^2}{2M_N E y} \approx A x_A$. The plots show the beam spin asymmetry $A_{LU}(\phi)$ (a), the $\sin\phi$ moment of A_{LU} as a function of x_B (b), $-\Delta^2$ (c), and $\mathcal{Q}^2$ (d) [without evolution] for the scattering of an electron on a deuteron target at $E_e = 6$ GeV. The kinematical variables are $x_B = 0.2$ (± 0.02), $\mathcal{Q}^2 = 1.5$ (± 0.3) GeV^2, and $\Delta^2 = -0.25$ (± 0.05) GeV^2, as appropriate in each sub plot.

The four models are [MUEL05]:

- A (dash-dotted): includes only $\mathcal{H}_1$;
- B (dashed): Model A, but with smaller sea-quark contribution;
- B$'$ (dotted): Model B, plus $\mathcal{H}_3$
- $\hat{B}$ (solid): Model B, plus $\mathcal{H}_5$;

The plots also show projected experimental error bars for $30 \times 24 = 720$ hours of beam time, for a beam polarization $P_e = 0.8$. The bin sizes are $\Delta Q^2 = 0.1$ GeV^2, $\Delta x_{Bj} = 0.04$, and $\Delta t = \Delta[\Delta^2] = 0.1$ GeV^2. In the actual experimental analysis, if the bin sizes are increased, the statistics per bin will improve. The plots in Fig. 5 are three 1-dimensional samples of the 3-D space (Δ^2, x_{Bj}, Q^2). The data will fill the full 3-D space within the limits in Fig. 5 with bins of comparable statistical precision.

As one can see in Fig. 5 there is a strong contribution to A_{LU} coming from $\mathcal{H}_3$ (cyan dotted curve of model B$'$). This reflects the large quadrupole form factor of the deuteron (see Eq. 10). Even though we cannot separate $\mathcal{H}_1$ and $\mathcal{H}_3$ in this experiment, our results will place stringent constraints on GPD models.

The error bars shown in Fig. 5 are based on the calculated numbers in Tab. 1. The table lists the projected beam spin asymmetry uncertainty ΔA_{LU} for all presented kinematic bins. The bin size in Q^2 is ± 0.3 GeV^2

(± 0.3 GeV^2 for panel d), in $-t$ it is ± 0.05 GeV^2 and in x_B it is ± 0.02. The table also lists the corresponding cross section σ integrated over each bin, the CLAS acceptance (section 7) and the expected total yield in number of events. Fig. 5 (d) shows a week Q^2 dependance of the beam spin asymmetry. By integrating over Q^2 we can reduce the errors for the x_B and t dependent measurement points of A_{LU} shown in Fig. 5 (b) and (c).

Q^2 GeV^2,	$-t$ GeV^2,	x_B	$\sigma[pb]$	acc.	yield	ΔA_{LU}
1.3	0.25	0.20	0.064	0.15	376	0.091
1.5	0.25	0.20	0.077	0.24	726	0.066
1.5	**0.25**	**0.20**	0.26	0.098	995	0.056
1.5	**0.35**	0.20	0.14	0.036	197	0.13
1.5	**0.45**	0.20	0.09	0.015	53	0.24
1.5	0.25	**0.25**	0.08	0.33	1030	0.055
1.5	0.25	**0.30**	0.04	0.14	213	0.12
1.5	0.25	**0.35**	0.025	0.024	23	0.37

Table 1: Projected beam spin asymmetry uncertainty ΔA_{LU} for all points shown in Fig. 5 as a function of Q^2, $-t$ and x_B, with corresponding integrated cross section σ, CLAS acceptance and expected total yield in number of events for 720 hours with a $\mathcal{L} = 1.5 \times 10^{34}$ $[\frac{1}{cm^2\, s}]$. The bin size in Q^2 is (± 0.1) GeV^2 in Fig. 5 (d) and (± 0.3) Fig. 5 (b) and (c), $-t$ (± 0.05) GeV^2, and x_B (± 0.02). The bold numbers for Q^2, $-t$ and x_B show the varied parameters in Fig. 5 (d), (c) and (b) respectively.

The model estimation of the beam spin asymmetry in coherent DVCS on a deuteron target was also given in [CANO04]. The s_1 and s_2 coefficients of the Fourier decomposition of $A_{LU} = a_0 + s_1 \sin\phi + s_2 \sin 2\phi$ as a function of -t and fixed values of $x_A = 0.2$, $Q^2 = 2$ GeV^2 and $E_e = 6$ GeV are presented in Fig. 6. As one can see there is a very sizable $\sin\phi$ moment at covered range of -t and non negligible $\sin 2\phi$ moment of A_{LU}. The beam spin asymmetry vanishes, with the square root $\sqrt{t_{min} - t}$, for $t = t_{min}$.

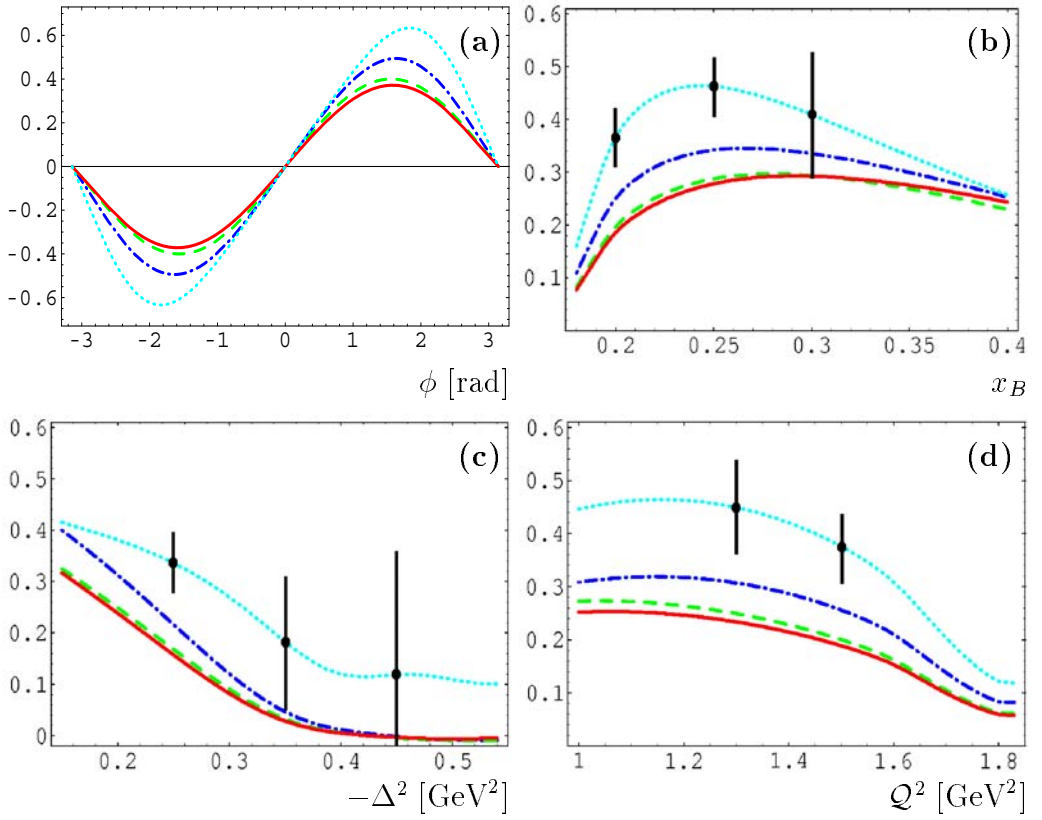

Figure 5: The beam spin asymmetry $A_{LU}(\phi)$ **(a)**, the $\sin\phi$ moment A_{LU} as function of x_B **(b)**, $-\Delta^2$ **(c)**, and $\mathcal{Q}^2$ **(d)** [without evolution] for the scattering of an electron on a deuteron target at $E_e = 6$ GeV. The average kinematical variables are $x_B = 0.2$, $\mathcal{Q}^2 = 1.5$ GeV^2, and $\Delta^2 = -0.25$ GeV^2 in panel (a). On panel (b), (c) and (d) two parameters are integrated over the range mentioned in the text and the third one varies. The models A (dash-dotted), B (dashed), $\hat{B}$ (solid), and B$'$ (dotted) are specified in the text of section 5. Error bars shown are based on 720 hours of beam time. For details see section 7.

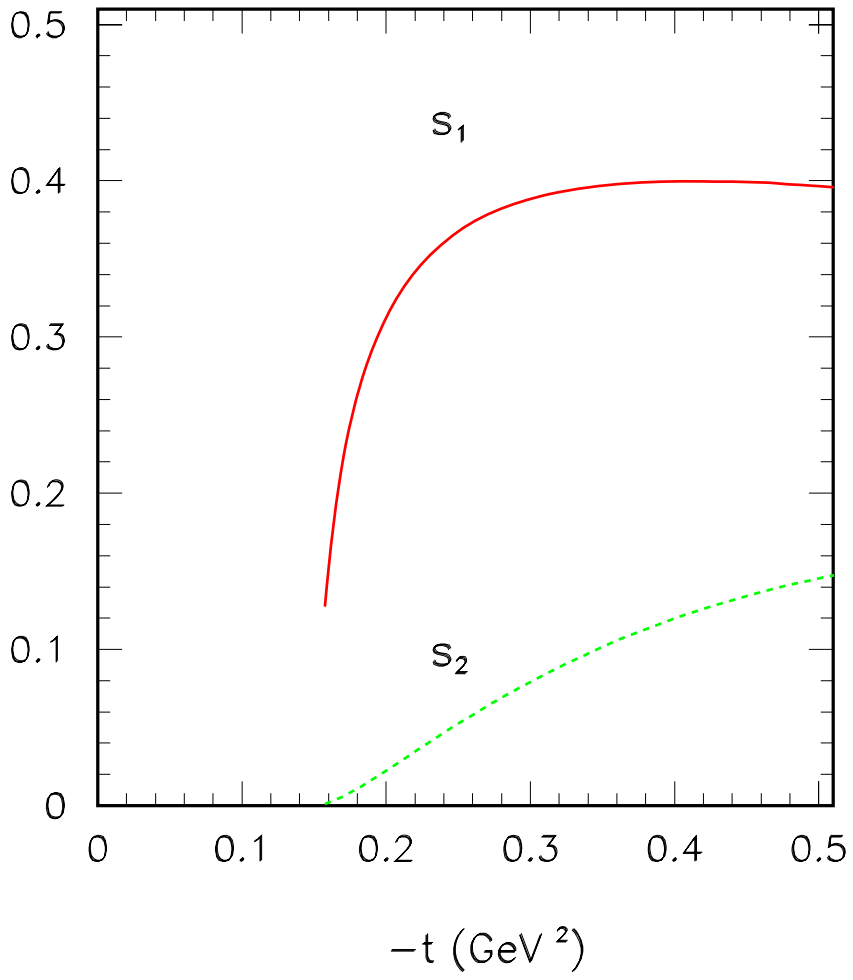

Figure 6: Coefficients of Fourier decomposition of the beam spin asymmetry: $A_{LU} = a_0 + s_1 \sin\phi + s_2 \sin 2\phi$ as a function of -t at $x_A = 0.2$, $Q^2 = 2$ GeV^2 and $E_e = 6$ GeV [CANO04].

6 Experimental DVCS Setup in Hall B

6.1 The DVCS CLAS configuration

We propose to use the same CLAS configuration as the approved PAC20 experiment E-01-113 (E1-DVCS), except for the production target. This configuration includes all standard CLAS detectors plus the inner calorimeter (IC), and also a solenoidal magnet for Møller electron background suppression. Instead of a liquid hydrogen target we propose to use a liquid deuterium target. The target length is 2.5 cm. All other components will remain unchanged.

6.1.1 Detectors

For this experiment we will have to utilize all available CLAS detectors, except for the tagging system, which is only used in photoproduction experiments. All detectors are standard CLAS components by now, except for the new IC. The experimental data can be grouped into coherent production and incoherent production. The detectors needed to identify both final states are very similar.

For the final state of the reaction $ed \to ed\gamma$ we have to detect

- the scattered electron (e) with threshold gas Čerenkov detectors (CC), drift chambers (DC) and forward electromagnetic calorimeters (EC)
- the recoil deuteron (d) with DC and time-of-flight scintillators (SC)
- the real photon (γ) with IC or EC

Fig. 7 (a) shows the particle identification with CLAS based on the measured β (time-of-flight) versus the measured momentum for π^+, proton and deuteron. The dashed line in Fig. 7 (b) indicates the minimum kinetic energy needed for deuteron detection with CLAS. In addition to time-of-flight for particle identification we can also utilize the measured energy loss of particles in the SC versus the measured momentum in the DC [CLAS02]. For incoherent production we have to detect the recoil proton instead of a deuteron.

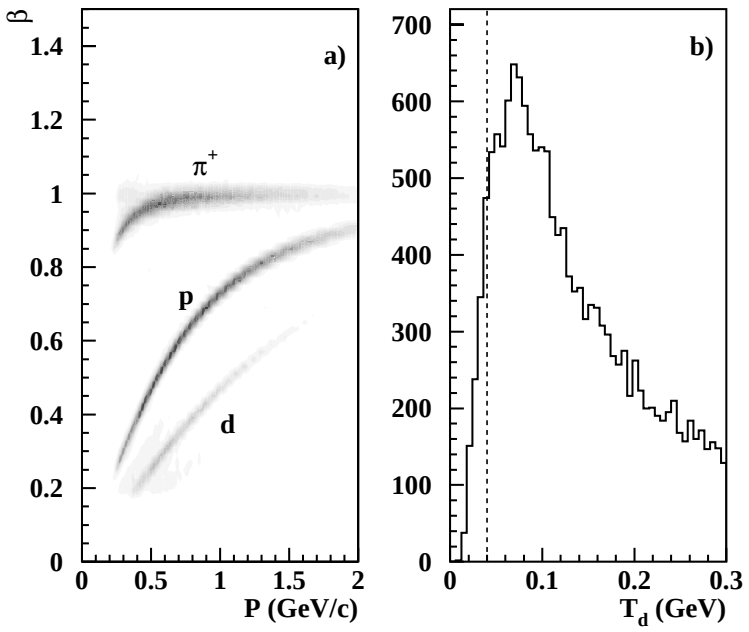

Figure 7: Time-of-flight based particle identification with CLAS (left) and minimum kinetic energy required for deuteron detection with CLAS indicated by a dashed line (right).

6.1.2 Møller electron shielding

This experiment, like all electroproduction experiments, has to address the background from Møller scattering. The cross section of this background is several orders of magnitude higher than the DVCS cross section. Background reduction will be done with the equipment chosen for the final design of experiment E1-DVCS. In particular the optimized lead shielding pipe and solenoidal magnetic field instead of the usual mini-torus shielding will be used against Møller electrons.

To achieve a central solenoid field of 4-5 T we use the CLAS superconducting solenoidal magnet. With this magnetic field Møller electrons are

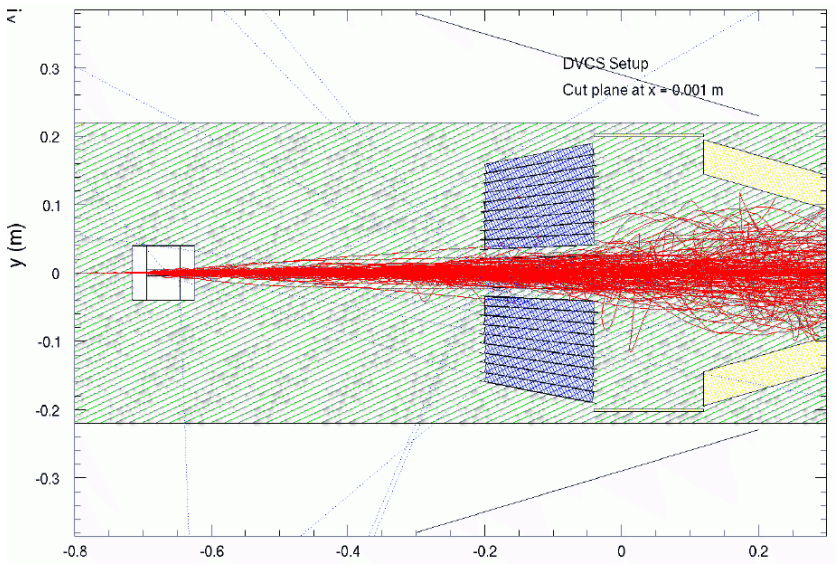

Figure 8: Simulated Møller electron distribution with solenoidal magnet installed, showing the target area and the IC along the beam line.

confined in a cone with a lab opening angle of about 2.5° at 1 m distance to the production target. The simulated Møller electron distribution with solenoidal magnet installed is shown in Fig. 8. The distribution illustrates the confinement of most Møller electrons along the beamline. The simulation gives us the number for the maximum luminosity $\mathcal{L} = 1.5 \times 10^{34}$ $[\frac{1}{cm^2\, s}]$. The same procedure has been used for prior experiments, including E1-DVCS.

6.1.3 Target

A liquid deuterium production target has been used before for other approved CLAS experiments, for example G2 and E1E. The target for this experiment will be located 12 cm downstream relative to the center of the solenoidal magnet, 58 cm upstream relative to the CLAS center. The solenoidal magnet will be at the same location as for E1-DVCS (z=-70cm). This configuration gives the best compromise between Møller suppression and deuteron acceptance. The accepted maximum angle Θ_{lab} for the deuteron is about 70°.

6.1.4 Inner calorimeter

One of the latest additions to the CLAS experiment is the inner calorimeter (IC) shown in Fig. 9. The IC is a lead tungstate $PbWO_4$ crystal array designed for the detection of high-energy photons. The angular range for photon detection is 4 to 16° in the lab system.

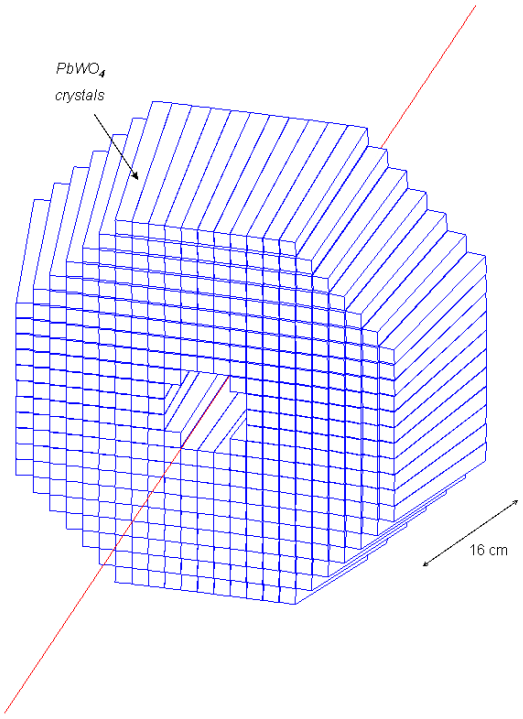

Figure 9: A view of the Inner Calorimeter (IC).

424 tapered crystals are arranged in a grid. Each crystal's cross section is 13.3 mm by 13.3 mm in the front and 16 mm by 16 mm in the rear. The length of each crystal is 160 mm, 18 times the radiation length L_0=8.9 mm.

The Molière radius is 22 mm. The lateral size of the crystals allows good position resolution due to the lateral spread of the shower across adjacent crystals.

The minimum energy for photons of interest is 1 GeV. Electromagnetic

showers from photons with an energy of 1 GeV or higher are typically confined within a group of about 3×3 crystals. The energy and position resolution, inferred both from simulation [GIRO05] and from data [NIYA05], are

$$\begin{aligned} \frac{\sigma E}{E} &= \frac{0.034}{E/1GeV} + \frac{0.038}{\sqrt{E/1GeV}} + 0.022 \ , \\ \sigma x &= \frac{0.18}{\sqrt{E/1GeV}} \, cm + 0.01 \ cm \ . \end{aligned}$$

The distance from the production target to the inner calorimeter (IC) is 60 cm. The IC is located in front of the lead shielding pipe. At this distance the expected lab angle resolution is approximately 5 mr at 1 GeV.

6.1.5 CLAS modifications

Fig. 10 shows the standard modifications of CLAS for DVCS runs. All parts are located inside the space covered by the drift chamber (DC) region 1. The inner calorimater (IC) can be seen downstream of the target and the solenoid magnet. Along the beam line follows the lead shielding pipe.

No other modifications of the CLAS apparatus are needed for the proposed experiment. No R&D work is required. The proposal fully benefits from recent developments for E1-DVCS.

The experiment can be ready in two weeks, including the installation and commissioning, if installation is needed and a few hours otherwise.

6.2 Trigger, data aquisition, online monitoring

We will use the CLAS electroproduction trigger, the CLAS data aquisition and the CLAS online monitoring. All three components are standard CLAS configurations. The CLAS level 1 trigger selects events with scattered electrons. We utilize the EC for this purpose and record in addition data from the CC for offline analysis. The level 2 trigger selects events with an additional charged particle. Both trigger levels will be utilized. No changes to the trigger hardware, data aquisition system or online monitoring are required.

The inner calorimeter (IC) will not be part of the trigger for production runs. The CLAS data aquisition system can handle the rate at acceptable

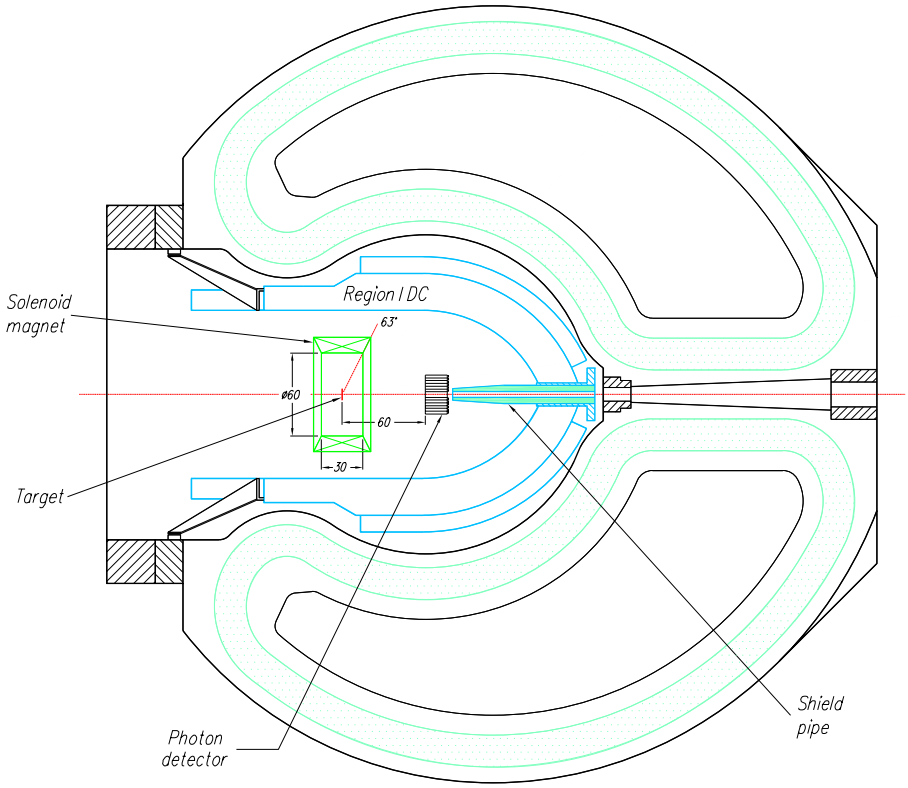

Figure 10: A cross section of CLAS. showing the main torus, the drift chamber region 1, the inner calorimeter, solenoid magnet and the lead shielding pipe.

dead time (better than 80%). The open trigger allows us to utilize production data for calibration purposes and to perform cross-checks with data from other well known reactions.

In addition, we will use the inner calorimeter (IC) alone in the trigger for IC calibration runs. This configuration has been used before in E1-DVCS and allows us to take sufficient IC calibration data within a time period of only 2 hours.

6.3 Calibration

The calibration of the detectors will be done with calibration data taken during the proposed experiment and using production data as well. The CLAS calibration software exists for all detectors. Therefore the calibration will begin immediately while data are being taken. This ensures data quality.

Electrons from any reaction with charged particles in the final state, to fulfill the trigger condition, can by used to calibrate the CC.

The DC calibration can be performed with protons from incoherent production.

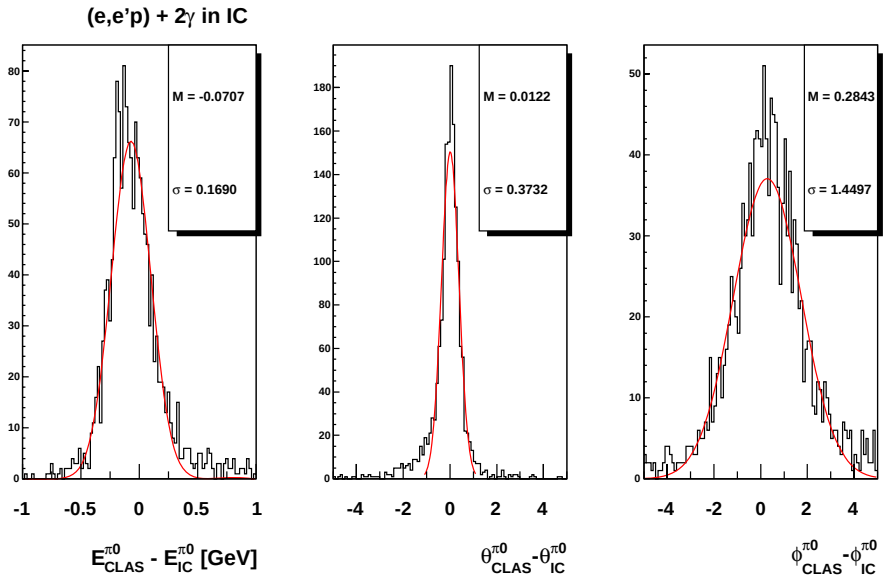

Figure 11: Energy and angular resolution of the Inner Calorimeter (IC), folded with CLAS missing mass and angular resolution.

The calorimeters EC, IC and LAC can be calibrated with the photons from decay of π^0's produced in the reaction $ed \rightarrow e\pi^0$ X . The energy resolution of the Inner Calorimeter (IC) is shown in Fig. 11.

6.4 IC monitoring

The light output of lead-tungstate crystals is sensitive to the ambient temperature. A laser driven fiber optics calibration system will be used to inject a controlled amount of light into the crystals via quartz fibers. The response will be recorded and used to determine the gain. This allows us to monitor the stability of crystal responses. Furthermore, single-π^0 production data can be used to monitor the responses over time as well.

6.5 Event identification, reconstruction

We propose an exclusive measurement of the DVCS/BH processes. All particles in the final state will be detected, identified and their 4-momentum measured.

The momentum measurement for deuterons and protons with the main torus and drift chambers (DC) is identical and common procedure at CLAS. Particle identification and separation of protons and deuterons will be done with the CLAS time-of-flight scintillators (SC).

Negative charged pions and kaons will be rejected as deuteron candidates on the basis of their charge, which is obtained from their curvature in the drift chambers.

Positive charged pions and kaons will be separated from protons and deuterons with the time-of-flight method (SC). We may want to utilize the energy loss measurement in the scintillators (SC) as an additional criterion for the particle idenfication, but it is not a requirement for this experiment.

Electrons will be separated from heavier negatively charged particles, in particular pions and muons, using threshold gas Čerenkov detectors (CC) within the acceptance of the CC and the electromagnetic calorimeters (EC). In addition we utilize the large acceptance of the EC alone for electrons outside the smaller acceptance of the CC and distinguish between electrons and pions by utilizing the different energy deposit in the EC from these two particles. The momentum of the electron is reconstructed with standard CLAS software from the drift chamber data.

Neutrons will be separated from photons by a cut on the time-of-flight. In addition the expected 3-momentum of the neutron in the reaction $ed \to epn\gamma$ can be used to locate neutrons.

The expected background from two-gamma events, in particular from π^0

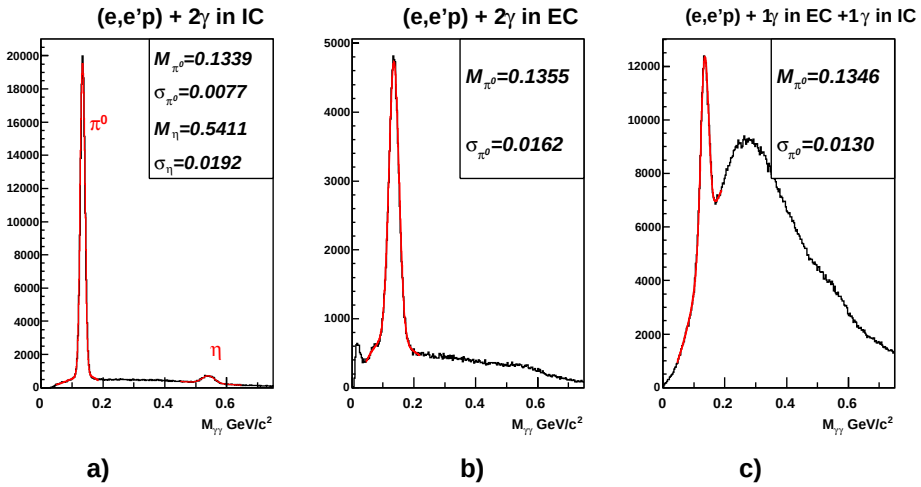

Figure 12: Mass resolution of π^0 in IC, EC and IC+EC.

production is expected to be as low as for the approved DVCS experiments at CLAS on the proton. The π^0 mass resolution is shown in Fig. 12.

All CLAS software needed for the event identification and reconstruction already exists. No modifications are required.

7 Simulations and Count Rates

In order to estimate the count rates and projected physics results for the proposed experiment we utilize a complete GEANT simulation of CLAS, called GSIM. GSIM includes detailed descriptions of all detectors (CC, DC, EC, LAC, SC and IC) as well as the target, magnets, the beam line and all relevant materials. Detector responses are simulated down to the level of ADC and TDC data, based on the most recent calibration constants from actual experiments, mostly E1-DVCS which is currently being analyzed by the collaboration. Physical effects such as multiple scattering, energy loss, secondary reactions etc. were all simulated, too.

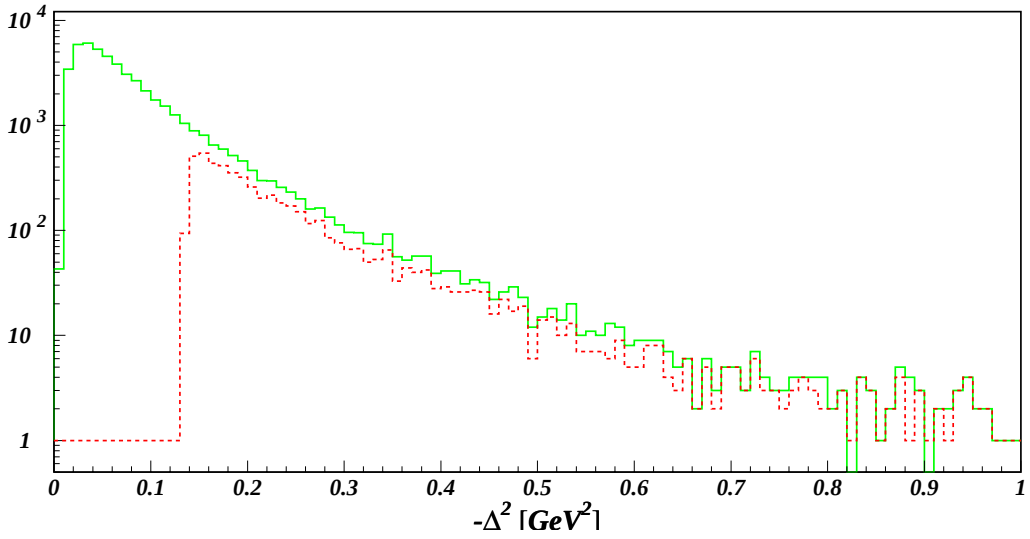

Figure 13: Expected distributions of events as function of Δ^2 (top left) for $\Delta^2 = 0.0 \ldots 1.0$ [GeV^2]. The plot shows the simulated distribution without CLAS (solid, green) and with detected deuteron (dashed, red).

We first determine the kinematical range needed for our simulation. Fig. 13 shows the Δ^2 distribution from the event generator and the smaller fraction of events where the deuteron has been detected by CLAS. No deuterons

are detected for $\Delta^2 < 0.13$ GeV^2. This is due to the minimum momentum needed for the deuteron to reach the time-of-flight (SC) detector. Therefore for all subsequent calculations we require $\Delta^2 \geq 0.13$ GeV^2. We also require $Q^2 \geq 1.0$ GeV^2. The acceptance shown in Fig. 13 does not change much with Δ^2 above $\Delta^2 \geq 0.13$ GeV^2. It does however change with the scattering angle Θ_d of the deuteron as expected. Most deuterons are scattered at a large angle Θ_d, where the acceptance is high.

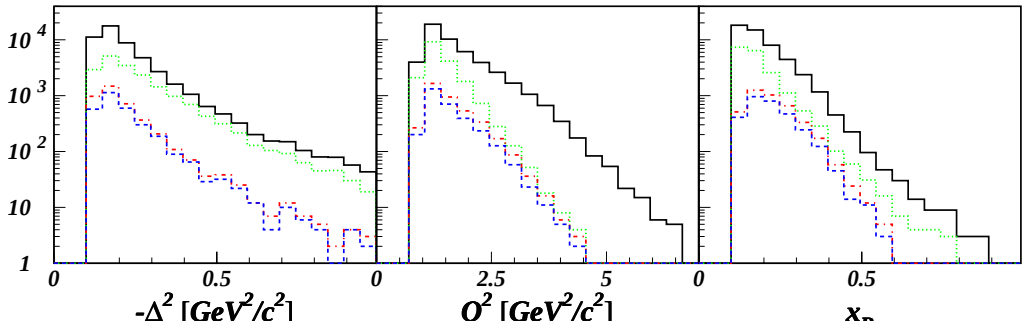

Figure 14: CLAS acceptance as a function of Δ^2 (left), Q^2 (center) and x_B (right) for $\Delta^2 = 0.13 \ldots 1.0$ [GeV^2], $Q^2 = 1.0 \ldots 7.0$ [GeV^2], and $x_B \geq 0.15$. Each plot shows the simulated distribution without CLAS (solid, black), with detected electron (dotted, green), plus detected photon (dash-dotted, red) and also with the detected deuteron (dashed, blue).

In a subsequent iteration the CLAS acceptance as function of Δ^2, Q^2, x_B and W has been determined. The result is shown in Fig. 14. All particles and detectors are now included. The following kinematical cuts were applied so that only events in the interesting range of this experiment were simulated:

- $\Delta^2 = 0.13 \ldots 1.0$ GeV^2,
- $Q^2 = 1.0 \ldots 7.0$ GeV^2, and
- $x_B \geq 0.15$.

Based on the simulation we estimate the number of Bethe-Heitler plus DVCS events per hour. The numbers are summarized in Tab. 1. For E1-DVCS the achieved luminosity was $\mathcal{L} = 2.0 \times 10^{34}$ $[\frac{1}{cm^2\,s}]$. Additional material from the target cell and windows did reduce the effective luminosity to about $\mathcal{L}_{eff} = 1.6 \times 10^{34}$ $[\frac{1}{cm^2\,s}]$. For this proposal on the deuteron target we assume a luminosity of $\mathcal{L}_{eff} = 1.5 \times 10^{34}$ $[\frac{1}{cm^2\,s}]$. We assume a beam polarization $P_e = 0.8$, which was achieved during the E1-DVCS experiment. We then calculate projected errors of the beam spin asymmetry measurement. For the errors shown in Fig. 5 a total of 720 beam hours are required. These error bars are calculated in the kinematical range used for the theoretical calculations. Of course, additional measurements at different combinations of Q^2, x_B and Δ^2 will come from the experiment, too. This measurement allows us to distinguish model B', which includes H_3 contribution, from the other models.

8 Summary

We propose to measure the beam-spin asymmetry in coherent Deeply Virtual Compton Scattering on the deuteron. This measurement will provide:

- First access to the GPDs of a spin-1 object in a linear combination of the $\mathcal{H}_1$, $\mathcal{H}_3$, and $\mathcal{H}_5$ functions in the x_{Bj}, t and Q^2 phase space;
- First direct sensitivity to the $\mathcal{H}_3$ GPD that is related to the quadrupole form factor of the deuteron.
- First access to the partonic structure, in coordinate and momentum space, of the deuteron as a coherent object.

These measurements combine the physics sensitivity of Deep Inelastic and Elastic Scattering on the composite nuclear system.

In addition to the coherent $D(e, e'D\gamma)$ channel, we will also measure incoherent $eD \to e'\gamma pn$ reaction as by-product of this proposal. As a function of momentum transfer to the proton or neutron, the incoherent process is primarily sensitive to either the proton or neutron GPDs. In the case of the proton, the comparison with Hydrogen data is a test of EMC effects on GPDs in the deuteron. Count rates for $D(e, e'\gamma p)n$ events will be much larger than the projections presented here for coherent DVCS, due to the large relative magnitude of the cross sections.

Our beam request is for 30 days of 6 GeV beam with a minimum polarization of 80%. We will use the standard CLAS configuration with a liquid Deuterium target (Luminosity $1.5 \times 10^{34}/\mathrm{cm}^2/\mathrm{s}$) supplemented with the target solenoid and the $PbWO_4$ Inner Calorimeter.

9 Acknowledgement

- U.S. National Science Foundation under grant no. PHY-0456520 (from D. Müller)

References

[AMAR00] M. Amarian, Deeply Virtual Compton Scattering at HERMES, 14th International Spin Physics Symposium (SPIN 2000), Osaka, Japan, Oct 16-21 2000, [http://www-hermes.desy.de/notes/pub/00-LIB/amarian.SPIN2000.proc.ps.gz].

[BELI01] A. Belitsky, D. Müller, L. Niedermeier, A. Schäfer, Nucl. Phys. B **593**, 289 (2001).

[BERG01] E. R. Berger, F. Cano, M. Diehl, B. Pire, Phys. Rev. Lett. **87**, 142302 (2001), [arXiv:hep-ph/0106192].

[BURK02] M. Burkardt, Int. J. Mod. Phys. A **18**, 173-208 (2003), [arXiv:hep-ph/0207047].

[CANO04] F. Cano and B. Pire, Eur. Phys. J. A **19**, 423-438 (2004).

[CLAS02] V. Burkert *et al.*, Charged Particle Identification in Electron Scattering Experiments with CLAS, CLAS-NOTE 02-006, 2002, [http://www.jlab.org/Hall-B/notes/clas_notes02.html].

[ELLI03] F. Ellinghaus *et al.* [HERMES Collaboration], Deeply-Virtual Compton Scattering on Deuterium and Neon at HERMES, 15th International Spin Physics Symposium (SPIN02), Brookhaven National Lab, NY, USA, Sep 9-14, 2002, AIP Conf. Proc **675**, 303 (2003), [arXiv:hep-ex/0212019].

[GARC01] M. Garçon and J. V. Orden, The deuteron: structure and form factors, Adv. Nucl. Phys. **26**, 293 (2001), [arXiv:nucl-th/0102049] (2001).

[GILM01] R. Gilman, F. Gross, Electromagnetic structure of the deuteron, J. Phys. G **28**, R37-R116 (2002), [arXiv:nucl-th/0111015] (2001).

[GIRO05] F.-X. Girod and M. Garçon, CLAS-Note 2005-001.

[H105] A. Aktas *et al.*, Eur. Phys. J. C **44**, 1-11 (2005).

[HAAN05] S. Haan, "Deeply Virtual Compton Scattering on Neon", Master thesis, Univ. Leibzig, Aug. 2005.

[HERM01] A. Airapetian *et al.*, Phys. Rev. Lett. **87**, 182001 (2001).

[HOFS57] R. Hofstadter, Ann. Rev. Nucl. Part. Sci. **7**, 231 (1957).

[JI97] X. Ji, Phys. Rev. D **55**, 7114 (1997).

[JI04] X. Ji, Ann. Rev. Nucl. Part. Sci. **54**, 413-450 (2004).

[KIRC03] A. Kirchner and D. Mueller, Eur. Phys. J. C **32**, 347 (2003) [arXiv:hep-ph/0302007].

[KRAU05] B. Krauss *et al.* [HERMES Collaboration], Recent HERMES Results on DVCS, [arXiv:hep-ex/0505016].

[LIUT05] S. Liuti and S. Taneja, Phys. Rev. C **72**, 032201 (2005).

[MUEL94] D. Müller, D. Robaschik, B. Geyer, F.-M. Dittes, J. Hořejši, Fortschr. Phys. **32**, 101 (1994).

[MUEL05] D. Müller, private communications, based on [KIRC03].

[NESS97] F. Nessi-Tedaldi, CMS conference report, represented at Beauty'97, 5th International workshop on B-Physics at Hadron machines, Los Angeles (USA), 13-17 October 1997.

[NIYA05] R. Niyazov and S. Stepanyan, CLAS-Note 2005-021.

[POLY03] M.V. Polyakov, Phys. Lett. B **555**, 57-62 (2003).

[RADY96] A. Radyushkin, Phys. Lett. B **380**, 417 (1996).

[RIED05] C. Riedl, "First Measurement of the Tensor Structure Function b_1^d of the Deuteron with the HERMES Experiment", Dr. thesis, July 2005; A. Airapetian *et al.*, [arXiv:hep-ex/0506018].

[SABA05] F. Sabatié, preliminary E6 analysis.

[SCOP04] S. Scopetta, [arXiv:nucl-th/0404014], [arXiv:nucl-th/0410057], [arXiv:nuc-th/0412107].

[STEP01] S. Stepanyan *et al.*, Phys. Rev. Lett. **87**, 182002 (2001).

[STRI03] V. Guzey and M. Strikman, Phys. Rev. C **68**, 015204 (2003).

[STRI04] A. Freund and M. Strikman, Eur. Phys. J. C **33**, 53-61 (2004).

[ZEUS03] S. Chekanov *et al.*, Phys. Lett. B **573**, 46-62 (2003).

List of Figures

1 "Handbag" diagram for DVCS. In the $ed \to ed\gamma$ reaction, the DVCS amplitude interferes with the Bethe-Heitler amplitude. 5

2 Beam spin asymmetry A_{LU} for $e^{\pm}d \to e^{\pm}\gamma X$ with unpolarized deuteron (a) and $e^{\pm}Ne \to e^{\pm}\gamma X$ (b) from HERMES, inclusive measurement [ELLI03, KRAU05]. 13

3 Missing mass m_X^2 of e d $\to$ e d X in GeV^2 for the ϕ bin averaged around 40° along with a skewed-gaussian + polynomial fit. . 14

4 Uncorrected beam spin asymmetry A_{LU} as a function of ϕ for $< x_A >= 0.1$, $< Q^2 >= 1.7$ GeV^2, $< -t >= 0.3$ GeV^2. The curve is a fit of the data with the function $\alpha \sin\phi + \beta \sin 2\phi$. . 16

5 The beam spin asymmetry $A_{LU}(\phi)$ **(a)**, the $\sin\phi$ moment A_{LU} as function of x_B **(b)**, $-\Delta^2$ **(c)**, and $\mathcal{Q}^2$ **(d)** [without evolution] for the scattering of an electron on a deuteron target at $E_e =$ 6 GeV. The average kinematical variables are $x_B = 0.2$, $\mathcal{Q}^2 =$ 1.5 GeV^2, and $\Delta^2 = -0.25$ GeV^2 in panel (a). On panel (b), (c) and (d) two parameters are integrated over the range mentioned in the text and the third one varies. The models A (dash-dotted), B (dashed), $\hat{B}$ (solid), and B$'$ (dotted) are specified in the text of section 5. Error bars shown are based on 720 hours of beam time. For details see section 7. 19

6 Coefficients of Fourier decomposition of the beam spin asymmetry: $A_{LU} = a_0 + s_1 \sin\phi + s_2 \sin 2\phi$ as a function of -t at $x_A = 0.2$, $Q^2 = 2$ GeV^2 and $E_e = 6$ GeV [CANO04]. 20

7 Time-of-flight based particle identification with CLAS (left) and minimum kinetic energy required for deuteron detection with CLAS indicated by a dashed line (right). 22

8 Simulated Møller electron distribution with solenoidal magnet installed, showing the target area and the IC along the beam line. 23

9 A view of the Inner Calorimeter (IC). 24

10 A cross section of CLAS. showing the main torus, the drift chamber region 1, the inner calorimeter, solenoid magnet and the lead shielding pipe. 26

11 Energy and angular resolution of the Inner Calorimeter (IC), folded with CLAS missing mass and angular resolution. . . . 27

12 Mass resolution of π^0 in IC, EC and IC+EC. 29
13 Expected distributions of events as function of Δ^2 (top left) for $\Delta^2 = 0.0 \ldots 1.0$ [GeV^2]. The plot shows the simulated distribution without CLAS (solid, green) and with detected deuteron (dashed, red). 30
14 CLAS acceptance as a function of Δ^2 (left), Q^2 (center) and x_B (right) for $\Delta^2 = 0.13 \ldots 1.0$ [GeV^2], $Q^2 = 1.0 \ldots 7.0$ [GeV^2], and $x_B \geq 0.15$. Each plot shows the simulated distribution without CLAS (solid, black), with detected electron (dotted, green), plus detected photon (dash-dotted, red) and also with the detected deuteron (dashed, blue). 31

List of Tables

1 Projected beam spin asymmetry uncertainty ΔA_{LU} for all points shown in Fig. 5 as a function of Q^2, $-t$ and x_B, with corresponding integrated cross section σ, CLAS acceptance and expected total yield in number of events for 720 hours with a $\mathcal{L} = 1.5 \times 10^{34}$ $[\frac{1}{cm^2\, s}]$. The bin size in Q^2 is ($\pm$0.1) GeV^2 in Fig. 5 (d) and ($\pm$0.3) Fig. 5 (b) and (c), $-t$ ($\pm$0.05) GeV^2, and x_B ($\pm$0.02). The bold numbers for Q^2, $-t$ and x_B show the varied parameters in Fig. 5 (d), (c) and (b) respectively. . 18